

# How does the length of the filars in a bifilar pendulum affect its period?

Personal code: XXXXXXXXXX

## 1 Introduction

A bifilar pendulum refers to a rigid body suspended by two strings, gyrating along its centre of mass. It is widely used to measure the moment of inertia of objects, which quantifies the amount of torque required to cause a specific angular acceleration along an axis. By observing the minute irregularities in the moment of inertia of the Earth, geologists can measure seismic events in remote locations, changes in the Earth's magnetic inclination and the effect of tides on the Earth's gravitational acceleration (Davison, 1894). Due to its high accuracy, bifilar pendulums are now used to measure the moment of inertia of complex geometries, such as aircraft and ships that would otherwise be infeasible to solve by hand (Jardin and Mueller, 2007). Since the moment of inertia is a critical parameter to aerodynamic and hydrodynamic stability, understanding the dynamics of a bifilar pendulum can lead to better designs in aircraft, enhancing the safety in transportation systems.

Although the general equation for bifilar pendulums has been well established, Klopsteg (1930) acknowledged the difficulty of determining the centre of mass of test objects, Kane and Tseng (1967) determined that minor inequalities of filar lengths will exhibit strong non-linear effects and chaotic side-sway motion, while Denman (1992) observed that torsional oscillations and vibrations in the filars cause significant deviations in the amplitude and period of bifilar pendulums. Given the wide range of unfulfilled assumptions and the variability of experimental results, the formulation of an accurate relationship will help solve real-life problems.

## 2 Framework

The following section aims to derive the equation of the bifilar pendulum, suspended by a rod (Amrozia and Muhammad, 2017; Then, 1965; Wouter, 2016):

$$T = \frac{\sqrt{3}\pi l_{rod}}{3r} \sqrt{\frac{l}{g}} \quad (1)$$

, where  $T$  is the period for one oscillation,  $l_{rod}$  is the length of the rod,  $l$  is the length of the filars,  $r$  is the radius of gyration and  $g$  is the acceleration due to gravity. Consider a bifilar pendulum with a rod  $MP$  suspended by filars  $AM$  and  $BP$ , disturbed from its equilibrium position  $MP$  to  $M'P'$  and allowed to oscillate about point  $O$  along the  $\hat{z}$  axis:

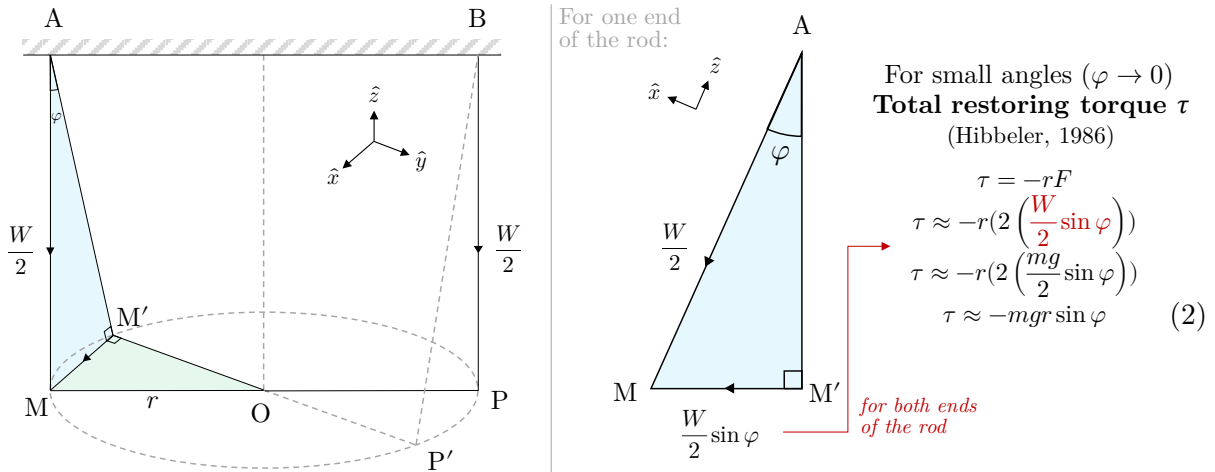


**Figure 1.** The decomposition of forces in a bifilar pendulum disturbed from its equilibrium position  $MP$ . (All diagrams are created by the candidate)

The total restoring torque  $\tau$  due to the weight of the rod  $W$  is obtained in (2). To better represent the motion of the rod, the relationship between  $\varphi$  and  $\theta$  is found to be:

For small angles ( $\theta \rightarrow 0, \varphi \rightarrow 0$ ):

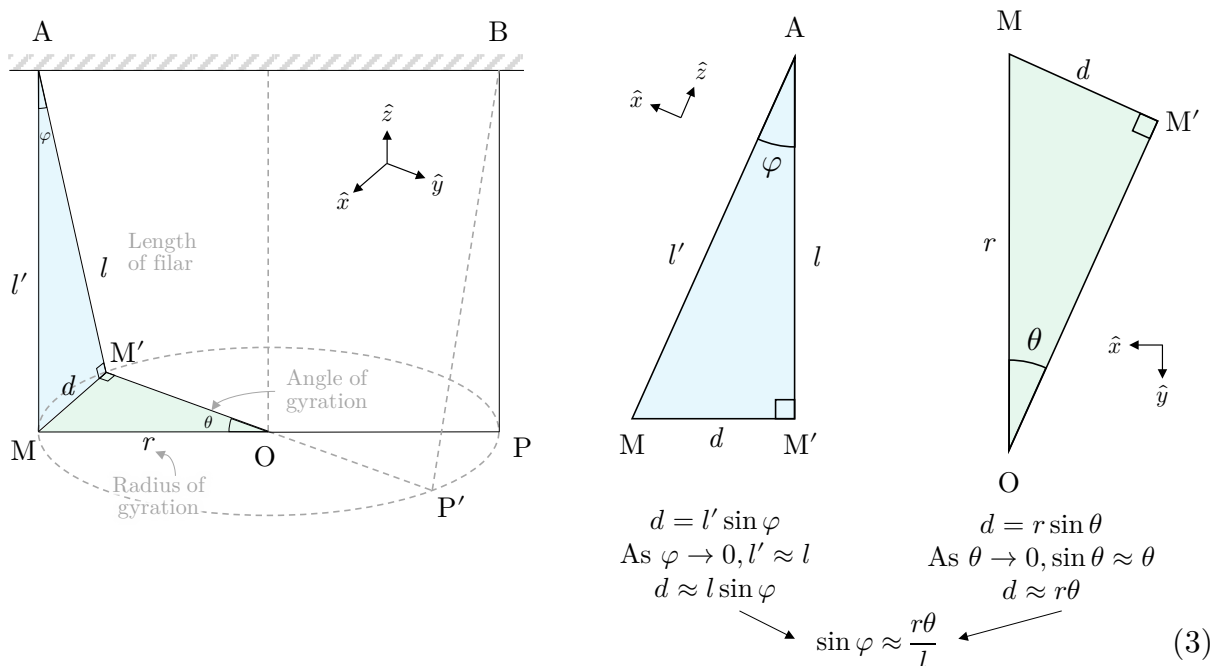


**Figure 2.** The approximate relationship between  $\varphi$  and  $\theta$  using trigonometric identities. Substituting (3) into (2), the total restoring torque  $\tau$  expressed in terms of  $\theta$  is:

$$\tau = -\frac{mgr^2\theta}{l} \quad (4)$$

Substituting (4) into Newton's Second Law of Angular motion yields (Hibbeler, 1986):

$$\begin{aligned} \tau &= I\ddot{\theta} \\ \ddot{\theta} + \frac{mgr^2}{Il}\theta &= 0 \end{aligned} \quad (5)$$

Solving the second-order differential equation in (5) with respect to time  $t$ , with initial angle  $\theta_i = \theta_0$  and initial angular velocity  $\dot{\theta}_i = 0$ , the solution is<sup>1</sup>:

$$\theta = \theta_0 \cos\left(\sqrt{\frac{mgr^2}{Il}}t\right) \quad (6)$$

Therefore, the period  $T$  of the cosine curve in (6) is:

$$T = \frac{2\pi}{\sqrt{\frac{mgr^2}{Il}}} = \frac{2\pi}{r} \sqrt{\frac{Il}{mg}} \quad (7)$$

The moment of inertia  $I$  of a slender cylindrical rod with length  $l_{rod}$  rotating about its centre of mass, along the  $\hat{z}$  axis is given by (Weisstein, 1996):

$$I = \frac{1}{12}ml_{rod}^2 \quad (8)$$

Substituting (8) into (7) and simplifying the equation yields the final relationship:

$$T = \frac{\sqrt{3}\pi l_{rod}}{3r} \sqrt{\frac{l}{g}} \quad (9)$$

<sup>1</sup> The full derivation of this differential equation can be found in the Appendix 17.1.

There are several required assumptions to support Equation 9:

1. The angle  $\theta$  is sufficiently small, such that the vertical translational kinetic energy is negligible when compared to the rotational kinetic energy, otherwise, the small-angle approximation will not hold, and increase the error in the period by the order of  $\mathcal{O}(\theta^3)$ .
2. There is no damping. Since  $\theta$  has an effect on  $T$ , the loss in rotational kinetic energy of the rod such as work done due to air resistance will decrease  $\theta$  and therefore decrease  $T$ .
3. The system has a high degree of symmetricity, namely the filars AM and BP are parallel to each other, have the same length  $l$  and aligned to the  $\hat{z}$  axis; the top AB and rod MP are parallel to each other, have the same length  $r$  and aligned to the  $\hat{x}$ - $\hat{y}$  plane. The axis of rotation should also pass through the midpoint and centre of mass of rod MP, otherwise slight deviations can amplify chaotic motion (Kane and Tseng, 1967).
4. There are no external forces that can cause lateral or vertical motion, ensuring stability.
5. The filars are assumed to be fully flexible, have no torsional rigidity and inextensible (Uhler, 1923). Microscopically, the strong intermolecular attraction between molecules of a particularly rigid filar will cause resistance to deformation, causing movements to require additional tension, resulting in damped responses and unpredictable motion.
6. The filars are massless, otherwise, it may cause the centre of mass of the test subject to be shifted upwards, decreasing the effective filar length  $l$  and increasing the mass  $m$ , overall decreasing the period of the oscillations (Karlin and Maday, 1985).

Additionally, Equation 9 can be linearised by expressing it in the slope-intercept form:

$$T = \underbrace{\frac{\sqrt{3}\pi l_{rod}}{3r}}_{\text{Plotted on y-axis}} \underbrace{\sqrt{\frac{1}{g}}}_{\text{Slope of graph}} \underbrace{\sqrt{l}}_{\text{Plotted on x-axis}} + \underbrace{0}_{\text{y-intercept}} \quad (10)$$

When  $T$  is plotted against  $\sqrt{l}$ , the slope and y-intercept is  $\frac{\sqrt{3}\pi l_{rod}}{3r} \sqrt{\frac{1}{g}}$  and 0 respectively.

### 3 Variables

Type	Name	Symbol	Description
Independent	Length of filars	$l$	This is measured using a metre ruler and further adjusted using the radii of rods to improve the accuracy. It is also ensured that the length is the same for both filars.
Dependent	Period	$T$	The time taken for the rod to oscillate one period. To reduce human bias and error, this is measured by semi-automatically extracting temporal changes of $\theta$ from a recording and deriving its period $T$ using Python scripts in Appendix 17.5 and 17.6.
Controlled	Radius of gyration	$r$	The distance between the axis of rotation and the filars. It is kept constant by securing the filar to a specific location on the rod using tape and to the top by wrapping around a capstan.
Controlled	Elastic strain energy	$U$	One of the mechanical properties of the filar. While Assumption 5 is hard to be fulfilled, by using the same filars across trials, the magnitude of the straining effect is kept constant and therefore predictable.
Controlled	Moment of inertia of rod	$I$	Quantifies the resistance of the test object against angular acceleration. This is kept constant by using the same test object and filars across all trials.

## 4 Pilot Study

As the percentage error in the period of the equation of the bifilar pendulum ( $T = \frac{\sqrt{3}\pi l_{rod}}{3r} \sqrt{\frac{l}{g}}$ ) is  $\frac{\Delta T}{T_0}$ , the denominator  $T_0$  must be sufficiently large to reduce the percentage error in  $T$ . There are three ways in which the range of the other variables can be adjusted to produce the least error:

1. Increasing the length of the rod ( $l_{rod}$ )
2. Increasing the length of the filars ( $l$ )
3. Decreasing radius of gyration ( $r$ )

As explored in Assumption 2, the loss in horizontal rotational kinetic energy should be minimised. Hence, to minimise the drag, a long slender rod with a low cross-sectional area of length  $l_{rod} = 0.1958 \pm 0.0001$  m and diameter  $d_{rod} = 0.00678 \pm 0.00001$  m has been selected as the test object.

However, if the radius of gyration ( $r$ ) is too low, the percentage error  $\frac{\Delta r}{r_0}$  will increase. Hence, a heatmap is created to better assess the effects of  $l$  and  $r$  on the percentage error of the period  $T$ :

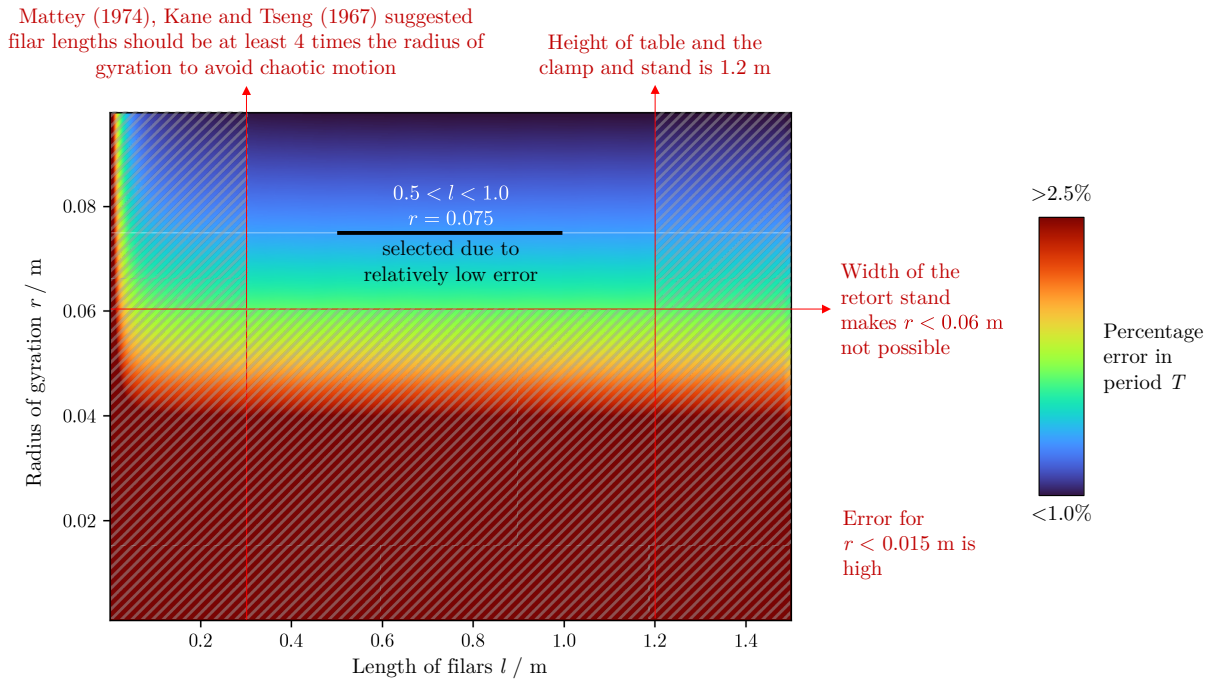


**Figure 3.** A heatmap of the percentage error in  $T$  for  $0 < l < 1.5$  s and  $0 < r < \frac{l_{rod}}{2}$  m.<sup>2</sup>

As observed in Figure 3, due to experimental setup limitations, the radius of gyration  $r$  is selected to be 0.0750 m. As for the range of the independent variable, length of filars  $l$ , it has been decided to perform 7 regular intervals between  $0.5 \leq l \leq 1.0$  m.

Moreover, because  $T \propto \sqrt{l}$ , when  $l \rightarrow \infty$ ,  $\frac{dT}{dl} \rightarrow 0$ , meaning that for increasing filar lengths, the corresponding magnitude of change in  $T$  is exponentially decreasing. Hence, in order to produce observable and significant changes in  $\Delta T$ , the length of filars  $l$  is controlled to be below 1.0 m, as demonstrated in Figure 4.

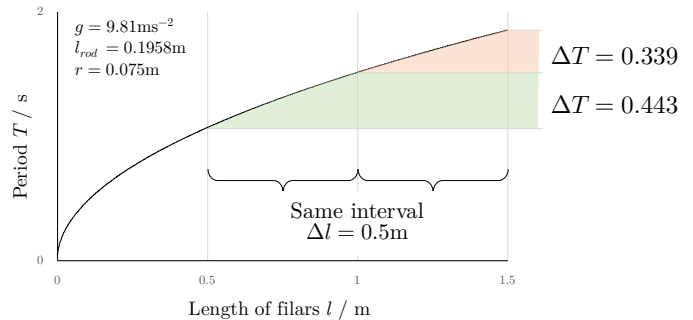


**Figure 4.** A graph of  $T$  against  $l$ .

<sup>2</sup> The relevant formulae and code used to generate the visualisation can be found in Appendix 17.2 and 17.3.

## 5 Apparatus

2x Clamp and stand	3x Metallic rod	1x Metre ruler ( $\pm 0.001\text{m}$ )
2x G-clamp	2x Cotton yarn	1x Vernier scale ( $\pm 0.0001\text{m}$ )
1x Tape	1x Camera	1x Micrometer ( $\pm 0.00001\text{m}$ )

## 6 Procedure and Precautions

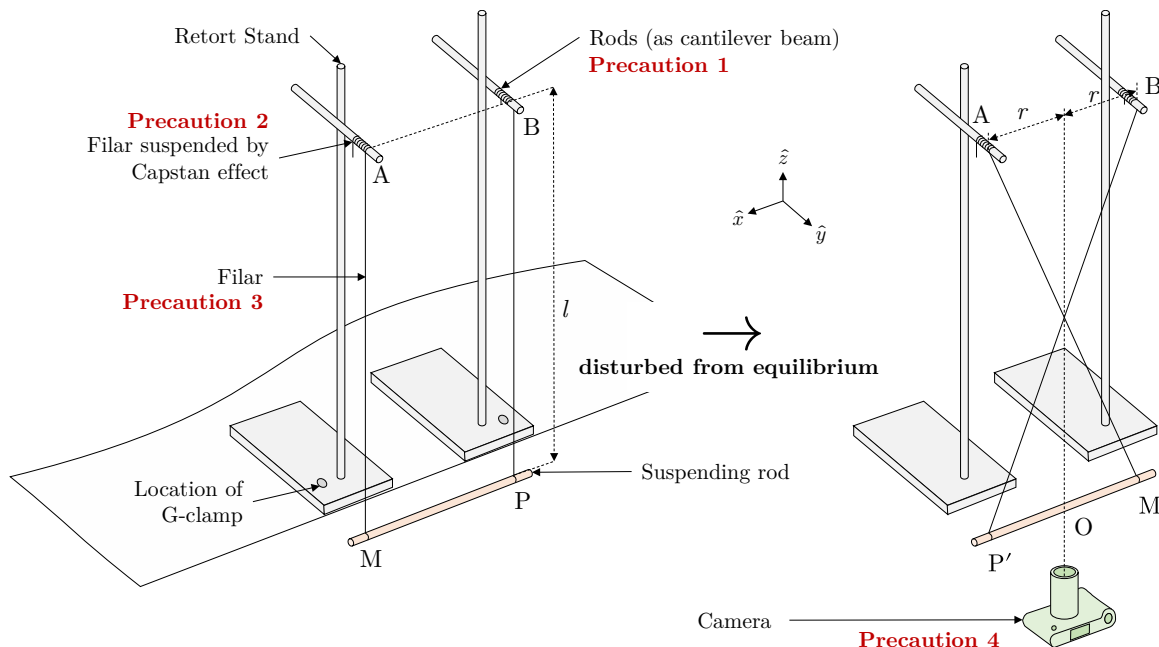


**Figure 5.** A diagram showing the setup of the experiment as rod MP is disturbed from its equilibrium.

1. Prepare and set up the apparatus accordingly to Figure 5.
2. Rotate rod MP clockwise to position  $M'P'$  such that filar AM comes in contact with filar BP, forming an angle of gyration  $\theta$  of  $\pi$ .
3. Release rod  $M'P'$  and allow it to rotate freely about O along the  $\hat{z}$  axis.
4. Start the recording when the angle of gyration  $\theta$  decreases to a small magnitude.
5. Stop the recording when the number of oscillations reaches 50.
6. Adjust the length of the filars  $l$  to the intervals by rotating the capstan at A and B.
7. Repeat steps 1-6 for three trials.

To reduce the possible sources of error, minimise the risk of accidents, and satisfy assumptions such as Assumption 3, there are several precautions marked in red in Figure 4:

1. Ensure that the top AB is level and aligned along the  $\hat{x}$  axis.
2. Ensure a high number of wraps around the capstan, increasing the limit of loading force.
3. Ensure that filars AM and BP have the same length  $l$  and are correctly aligned along the  $\hat{z}$  axis, especially during Step 6.
4. Ensure that the optical centre of the camera is colinear with O and the intersection of  $AM'$  and  $BP'$ , such that the distance between the midpoint of AB has the same radius  $r$ .

## 7 Ethical, safety and environmental concerns

Since the only waste product disposed of are cotton filars which are biodegradable (Li et al., 2010), there are no significant environmental or ethical concerns. Regarding safety concerns, there is a small risk where the filar at A and B loses traction, causing rod MP to fall and cause injury, but such a possibility has already been minimised by increasing the wrap count around the capstan.

## 8 Raw Data Table

Measured Length of Filars	Period			$T \pm \Delta T$ s $\pm$ s
	Trial 1	Trial 2	Trial 3	
$l_{raw}$ m	$T_1$ s	$T_2$ s	$T_3$ s	
$\Delta_{instrument} = 0.001\text{m}$	$\Delta T_1 = 0.0005\text{s}$	$\Delta T_2 = 0.0005\text{s}$	$\Delta T_3 = 0.0005\text{s}$	
0.494	1.0383	1.0387	1.0483	$1.04 \pm 0.01$
0.594	1.1165	1.1313	1.1226	$1.12 \pm 0.01$
0.654	1.1813	1.1957	1.2298	$1.21 \pm 0.02$
0.734	1.2643	1.2787	1.2876	$1.28 \pm 0.01$
0.814	1.3387	1.3522	1.3509	$1.35 \pm 0.01$
0.894	1.3850	1.4215	1.4072	$1.40 \pm 0.02$
0.974	1.4531	1.5052	1.4830	$1.48 \pm 0.03$

## 9 Qualitative Observation

During the experiment, the period is observed to increase as the length of the filars increase. However, several assumptions outlined in the framework appears to be violated. As an example, the vertical position of the rod M'P' is observed to be higher than its equilibrium position MP, causing a vertical motion of the rod along the  $\hat{z}$  axis. For small filar lengths, the effect is also observed to be very significant, meaning a loss in kinetic energy due to vertical motion, violating Assumption 1. Furthermore, with the angle of gyration and amplitude of motion dampening over time, this violates Assumption 2. Additionally, it has been observed that the pendulum exhibits strong sensitivity to minor changes in the inputs, often causing the centre of mass to sway horizontally unpredictably as it is released by hand, violating Assumption 3. As a result, when any of the above scenarios are believed to significantly impact the rotational motion, such trials are discarded and repeated.

## 10 Processed Data Table

Square root of length of filars	Absolute uncertainty in square root of length of filars	Period	Absolute uncertainty in period
$\sqrt{l}$ m $^{\frac{1}{2}}$	$\pm \Delta \sqrt{l}$ $\pm \text{m}^{\frac{1}{2}}$	$T$ s	$\Delta T$ $\pm \text{s}$
0.7029	0.0007	1.04	0.01
0.7576	0.0007	1.12	0.01
0.8087	0.0006	1.21	0.02
0.8568	0.0006	1.28	0.01
0.9022	0.0006	1.35	0.01
0.9455	0.0005	1.40	0.02
0.9869	0.0005	1.48	0.03

The following is a sample calculation when  $l_{raw} = 0.974$  m:

As the torque of the rotational motion originates from the centre of mass of the rod, the filar length  $l$  can be more accurately represented by accounting for the distance to the centre of mass. Hence, the measured length of filars  $l_{raw}$  is further offset using the respective radii of the rods<sup>3</sup>:

$$l = l_{raw} - \frac{1}{2}d_{top} + \frac{1}{2}d_{rod} \quad (11)$$

<sup>3</sup> A visualisation and derivation of the offset formula is provided in Appendix 17.4.

As explored in (10), the linearised form involves taking the square root of the filar length  $l$ . Substituting  $l_{raw} = 0.974$  m,  $d_{top} = 0.00678$  m and  $d_{rod} = 0.00683$  m into (11)<sup>3</sup>:

$$\sqrt{l} = \sqrt{l_{raw} - \frac{d_{top}}{2} + \frac{d_{rod}}{2}} = \sqrt{0.974 - \frac{0.00678}{2} + \frac{0.00683}{2}} = 0.9869 \text{ m}^{\frac{1}{2}} \text{ (4d.p.)} \quad (12)$$

Consider the representation of  $\sqrt{l}$  as a multivariable function  $f(l_{raw}, r_{top}, r_{rod})$ , then the formula for error propagation (Ku, 1966) can be used to find the absolute uncertainty in  $\sqrt{l}$ :

$$\begin{aligned} \Delta\sqrt{l} &= \sqrt{\left(\frac{\partial f}{\partial l_{raw}} \Delta l_{raw}\right)^2 + \left(\frac{\partial f}{\partial r_{top}} \Delta r_{top}\right)^2 + \left(\frac{\partial f}{\partial r_{rod}} \Delta r_{rod}\right)^2} \\ \Delta\sqrt{l} &= \sqrt{\left(\frac{\Delta l_{raw}}{2\sqrt{l_{raw} - \frac{r_{top}}{2} + \frac{r_{rod}}{2}}}\right)^2 + \left(-\frac{\Delta r_{top}}{4\sqrt{l_{raw} - \frac{r_{top}}{2} + \frac{r_{rod}}{2}}}\right)^2 + \left(\frac{\Delta r_{rod}}{4\sqrt{l_{raw} - \frac{r_{top}}{2} + \frac{r_{rod}}{2}}}\right)^2} \\ \Delta\sqrt{l} &= \sqrt{\left(\frac{0.001}{2\sqrt{0.974025}}\right)^2 + \left(-\frac{0.00001}{4\sqrt{0.974025}}\right)^2 + \left(\frac{0.00001}{4\sqrt{0.974025}}\right)^2} = 0.0005 \text{ m}^{\frac{1}{2}} \text{ (1s.f.)} \quad (13) \end{aligned}$$

As for the calculation of the dependent variable period  $T$ , the temporal change in the angle of gyration  $\theta(t)$  is first extracted from the recordings of the three trials and is then used to derive  $T$  by passing it through a series of automated computer instructions<sup>4</sup>. The advantage of utilising scripts to calculate variables is to minimise human reaction time errors and human bias.

For each trial, each frame of the recording is first passed through a Canny edge detector which produces an outline of the rod (Canny, 1986), then processed with a probabilistic Hough transform to extract the possible locations of the rod (Hough, 1962), as demonstrated below:

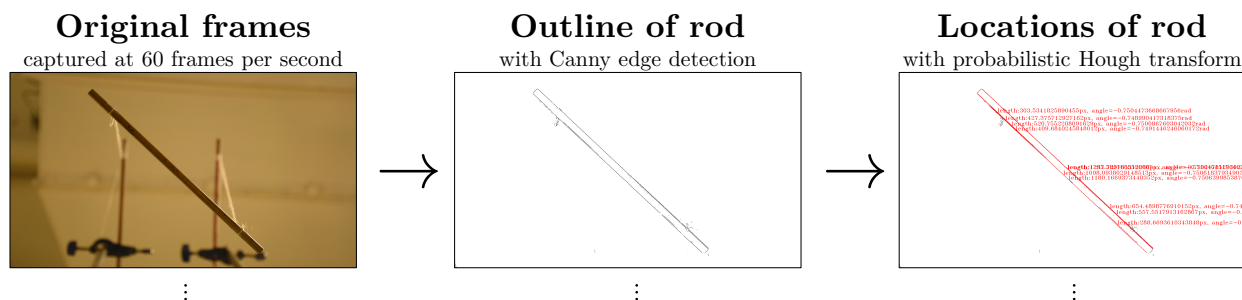


**Figure 6.** The process of extracting the possible locations of the rod from a recording.

Since longer Hough lines generally suggest a confident match (Matas et al., 2000), the angle of gyration is calculated using the endpoint coordinates  $(x_1, y_1)$ ,  $(x_2, y_2)$  of the longest Hough line:

$$\theta = \tan^{-1} \left( \frac{y_2 - y_1}{x_2 - x_1} \right) \quad (14)$$

From (6), a plot of the angle of gyration  $\theta$  against time  $t$  is expected to follow a cosine curve. Therefore, the average period of each oscillation  $T$  can be calculated by dividing the difference in time ( $\Delta t$ ) between the first and last maxima of  $\theta(t)$  by the number of oscillations  $n$ :

$$T = \frac{\Delta t}{n} = \frac{t_{45} - t_0}{45} \quad (15)$$

With reference to (15), the uncertainty in  $T$  is:

$$\Delta T = \sqrt{\left(\frac{\Delta t_{45}}{45}\right)^2 + \left(\frac{\Delta t_0}{45}\right)^2} \quad (16)$$

<sup>4</sup> The Python scripts used to perform the task can be found in Appendix 17.5 and 17.6 respectively.

Additionally, to improve the accuracy of the algorithm in selecting peaks, noisy data is first passed through a Savitzky-Golay filter (Savitzky and Golay, 1964), as demonstrated below:

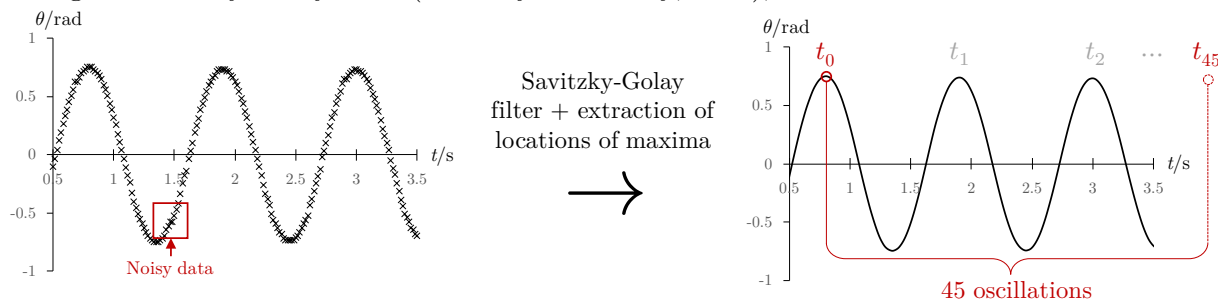


**Figure 7.** The process of smoothening the function of the angle of gyration  $\theta$  over time  $t$ .

Substituting in the values for Trial 1 into (15) and (16), the period  $T_1$  is therefore<sup>5</sup>:

$$T_1 = \frac{66.15 - 0.76}{45} \pm \sqrt{\left(\frac{1}{60}\right)^2 + \left(\frac{1}{45}\right)^2}$$

$$T_1 = 1.4531 \pm 0.0005 \text{ s (4d.p.)} \quad (17)$$

The half-range method is then used to obtain the average period across 3 trials:

$$T_{max} = \max(T_1 + \Delta T_1, T_2 + \Delta T_2, T_3 + \Delta T_3) = 1.51 \text{ s (2d.p.)}$$

$$T_{min} = \min(T_1 - \Delta T_1, T_2 - \Delta T_2, T_3 - \Delta T_3) = 1.45 \text{ s (2d.p.)}$$

$$T = \frac{T_{max} + T_{min}}{2} \pm \frac{T_{max} - T_{min}}{2} = 1.48 \pm 0.03 \text{ s (2d.p.)} \quad (18)$$

## 11 Graph

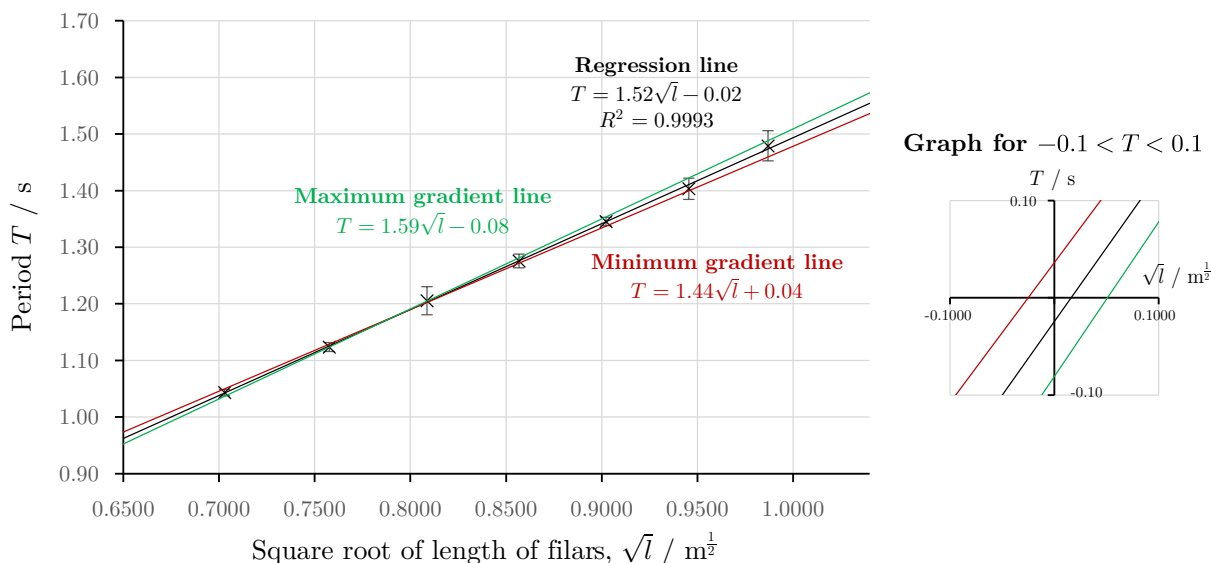


**Figure 8.** A linearised plot of the period ( $T$ ) against square root of length of filars ( $\sqrt{l}$ ).<sup>6</sup>

As shown in Figure 8, since the maximum and minimum gradient lines pass through the error bars of all points, it can be said that there are no significant anomalies. However, it has been observed that the absolute uncertainty in period for  $\sqrt{l} = 0.8087 \text{ m}^{\frac{1}{2}}$  is exceptionally large. Upon further inspection of the footage in Trial 3, a gust of wind has caused the axis of rotation to sway unpredictably at  $t \approx 104 \text{ s}$ , violating Assumption 3 and 4, potentially explaining why the period

<sup>5</sup> Since the recording has a framerate of 60 frames per second, the uncertainty in time  $\Delta T$  is  $\frac{1}{60} \text{ s}$ .

<sup>6</sup> As the greatest absolute uncertainty in  $\sqrt{l}$  is only  $\pm 0.0007 \text{ m}^{\frac{1}{2}}$ , when the horizontal error bar is plotted on the graph, it will only take up 0.179% of the horizontal space. Since this magnitude is too small to be observed, the horizontal error bars are not shown.



of oscillation is higher than expected. Regarding the goodness of fit for the line of best fit, as the magnitude of the error bars tend to increase as  $\sqrt{l}$  increases, it is possible to fit an exponential or logarithmic line of best fit. However, due to the small magnitude of the error bars, the only suitable type of line of best fit that fits appropriately within the bounds of the error bars is linear.

## 12 Conclusion

The best mathematical relationship between the two variables is: the period  $T$  is positively and directly proportional to the square root of the filar length  $\sqrt{l}$ . As demonstrated in (10), when  $T$  is plotted against  $\sqrt{l}$ , the expected slope is  $\frac{\sqrt{3}\pi l_{rod}}{3r} \sqrt{\frac{1}{g}}$  and the y-intercept is 0.

As shown in Figure 8, since the minimum gradient is  $1.44 \text{ sm}^{-\frac{1}{2}}$  and the maximum gradient is  $1.59 \text{ sm}^{-\frac{1}{2}}$ , the experimental gradient is therefore:

$$m = \frac{m_{max} + m_{min}}{2} \pm \frac{m_{max} - m_{min}}{2} = 1.52 \pm 0.07 \text{ sm}^{-\frac{1}{2}} \text{ (2d.p.)} \quad (19)$$

By rearranging the equation of the expected slope ( $m = \frac{\sqrt{3}\pi l_{rod}}{3r} \sqrt{\frac{1}{g}}$ ) and applying the formula for error propagation (Ku, 1966), the acceleration due to gravity  $g$  is:

$$g = \frac{\pi^2 l_{rod}^2}{3m^2 r^2} \pm \sqrt{\left(\frac{2\pi^2 l_{rod}}{3m^2 r^2} \Delta l_{rod}\right)^2 + \left(-\frac{\pi^2 l_{rod}^2}{6m^3 r^2} \Delta m\right)^2 + \left(-\frac{\pi^2 l_{rod}^2}{6m^2 r^3} \Delta r\right)^2} \quad (20)$$

Substituting (19),  $l_{rod} = 0.1958 \pm 0.0001 \text{ m}$ ,  $r = 0.0750 \pm 0.0001 \text{ m}$  into (20):

$$g = 9.8 \pm 0.2 \text{ ms}^{-2} \text{ (1d.p.)} \quad (21)$$

From above, since the measured gravitational acceleration is within the range of the theoretical value of  $9.81 \text{ ms}^{-2}$ , the experiment fits the general trend.

According to Krippendorff (1970), systematic error is defined as a constant deviation of values in a uniform direction. Hence, for the experiment to have an insignificant systematic error, the minimum and maximum gradient lines should encompass the origin. While it is common to quantify the magnitude of the systematic error in the period  $T$  by assessing the range of the y-intercept, because the period is computed using fully automated scripts, it is likely that the systematic error has instead evolved from human errors, such as the mismeasurements in the filar length  $l$ . Thus, it would be more meaningful to propagate the error in the period  $T$  (y-axis) to the filar length  $l$  (x-axis), such that the sources of the error can be clearly identified and mitigated in the future. This is done so by taking the half-range of the bounds of the x-intercepts:

$$\sqrt{l}_{error} = \frac{\sqrt{l}_{error_{max}} + \sqrt{l}_{error_{min}}}{2} \pm \frac{\sqrt{l}_{error_{max}} - \sqrt{l}_{error_{min}}}{2} = 0.01 \pm 0.03 \text{ m}^{\frac{1}{2}} \text{ (2d.p.)} \quad (22)$$

By taking the square on  $\sqrt{l}_{err}$ , the systematic error in the filar length is:

$$l_{error} = (\sqrt{l}_{error})^2 \pm 2(\Delta\sqrt{l}_{error})(\sqrt{l}_{error}) = 0.0002 \pm 0.0010 \text{ m (4d.p.)} \quad (23)$$

From (23), it can be said that the filar length  $l$  is on average overestimated by  $0.2 \pm 1.0 \text{ mm}$ . However, since this magnitude is very small and less than the smallest perceivable division on the measuring equipment ( $\pm 0.5 \text{ mm}$ ), the systematic error in  $l$  is overall insignificant and negligible. Therefore, it can be concluded that  $T$  is directly proportional to  $\sqrt{l}$ .

## 13 Comparison with Literature

In the equation of the bifilar pendulum ( $T = \frac{\sqrt{3}\pi l_{rod}}{3} \sqrt{\frac{l}{g}}$ ), the only variables that affect the

relationship are the length of the rod  $l_{rod}$ , the radius of gyration  $r$  and the gravitational acceleration  $g$ . Therefore, to test whether the results are reasonable, the theoretical period have been calculated using the literature values ( $l_{rod} = 0.1958 \pm 0.0001$  m,  $r = 0.0750 \pm 0.0001$  m,  $g = 9.81$  ms<sup>-2</sup>) and plotted onto Figure 9 below, to allow comparisons with the experimental data.

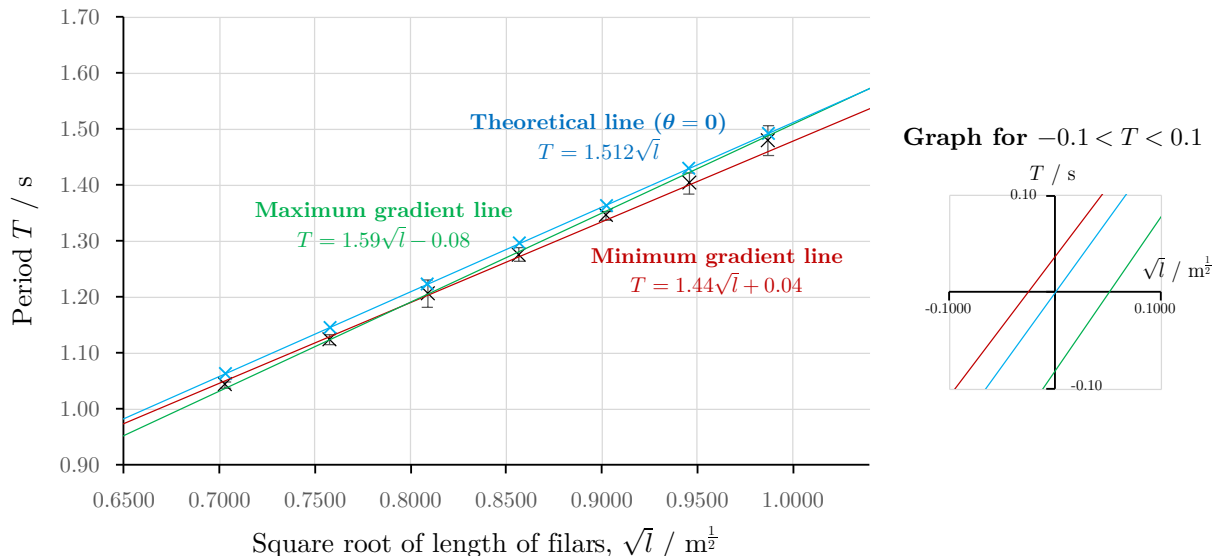


**Figure 9.** A linearised plot of the experimental and theoretical values of  $T$  against  $\sqrt{l}$ .<sup>7</sup>

As shown above, because the theoretical line only passes through the error bars of the third and last data point, it suggests that the data is only slightly reliable. It has also been observed that the experimental slope ( $1.52 \pm 0.07$  sm<sup>-1/2</sup>) is slightly greater than the theoretical slope ( $1.512 \pm 0.002$ sm<sup>-1/2</sup>). While this may have been explained by flaws in the physical properties in the apparatus, for example, the unequal mass distribution of the rod resulting to the overestimation in the moment of inertia, this speculation may be too superficial to be proven to be true within the errors of the currently available apparatus. Rather, it would be more appropriate to assess whether there are violations to the physical assumptions during the experimental process.

One of the major assumptions violated is Assumption 1, where the initial angle of gyration  $\theta_0$  is assumed to be zero. However, because the angle of gyration must be non-zero to cause some amount of observable motion, the period  $T$  is subsequently unavoidably greater than the theoretical since additional time is used to perform the vertical motion. To account for this, Karlin and Maday (1985), Khan et al. (2017) and Wouter (2016) proposed a non-linear representation of Equation 5, eliminating the use of small-angle approximations:

$$\ddot{\theta} + \frac{3gr^2 \sin \theta}{l_{rod}^2 \sqrt{l^2 - \frac{r^2(1 - \cos \theta)}{2}}} = 0 \quad (24)$$

By solving (24) using numerical methods,  $\theta(t)$  is approximated and the period  $T$  is subsequently derived from the average difference in  $t$  between the two maxima of  $\theta(t)$ ,<sup>8</sup> such that the theoretical values of the period  $T$  can be calculated for different initial values of gyration angles  $\theta_0$ .

As demonstrated in Figure 10 below, when the initial angle of gyration  $\theta_i$  is increased, the theoretical slope generally increases and no longer exhibits proportionality. This justifies why the

<sup>7</sup> As the greatest absolute uncertainty in the theoretical period  $T$  is only 0.002s, it will only take up 0.25% of the vertical space. Since this magnitude is too small to be observed, the vertical error bars are not shown.

<sup>8</sup>  $\theta(t)$  is approximated using numerical methods because it is infeasible to obtain the analytical solution of such a complex differential equation. The Python script used to perform the numerical method can be found in Appendix 17.7.

experimental slope is greater than the theoretical (when  $\theta_0$  is assumed to be zero):

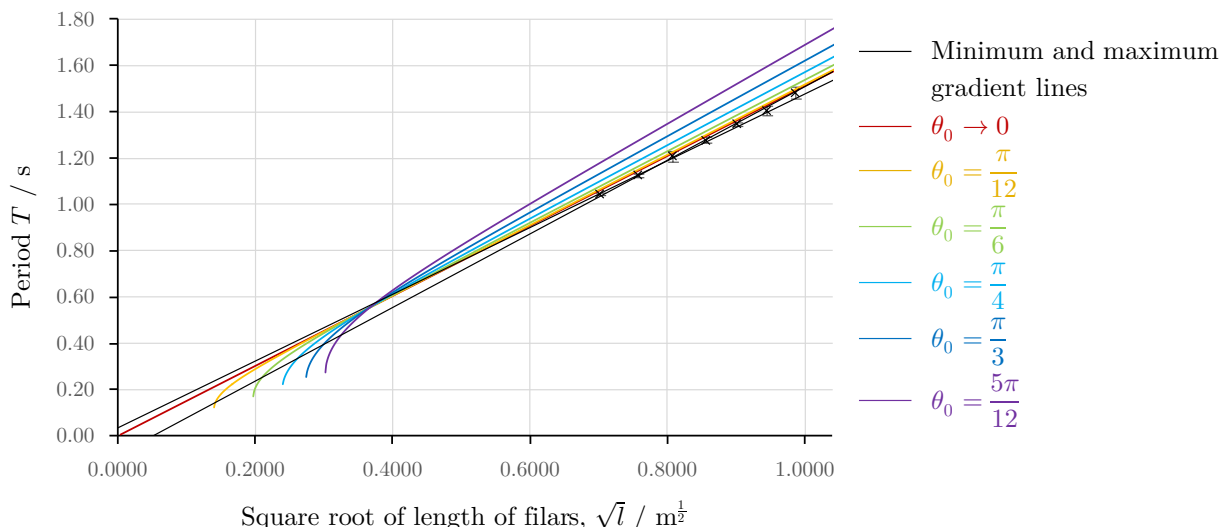


Figure 10. Theoretical values of  $T$  against  $\sqrt{l}$ , for varying initial angles of gyration  $\theta_0$ .

## 14 Sources of error and limitations

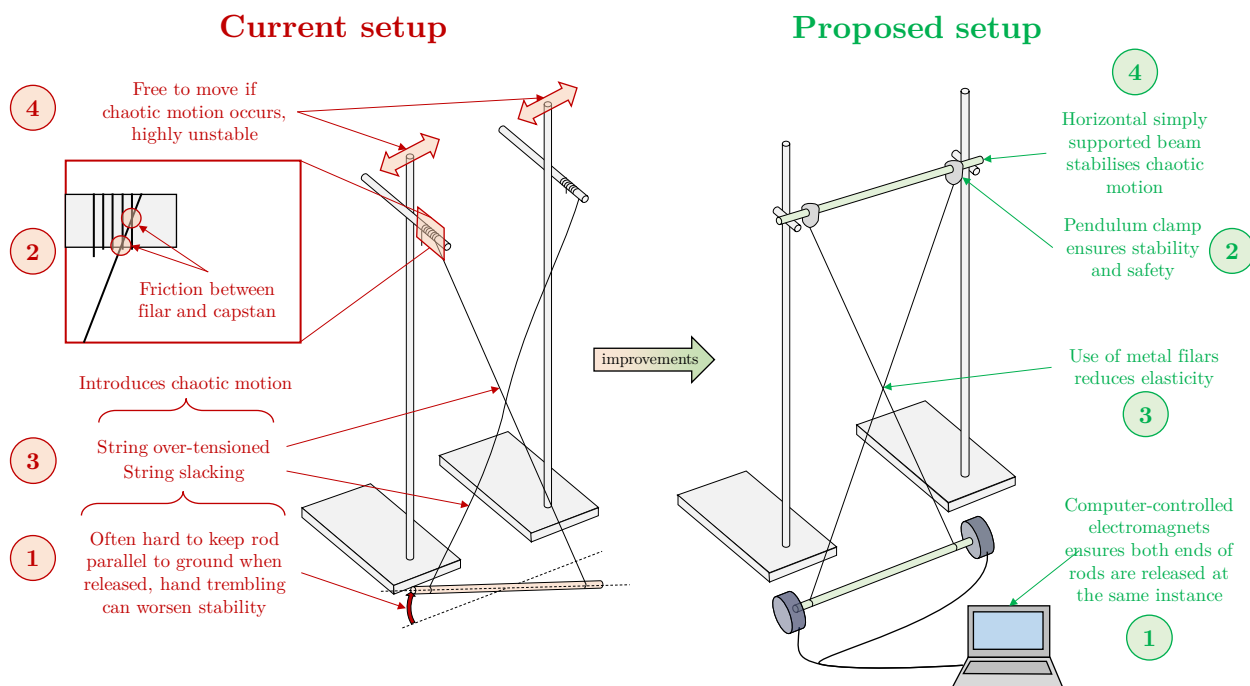
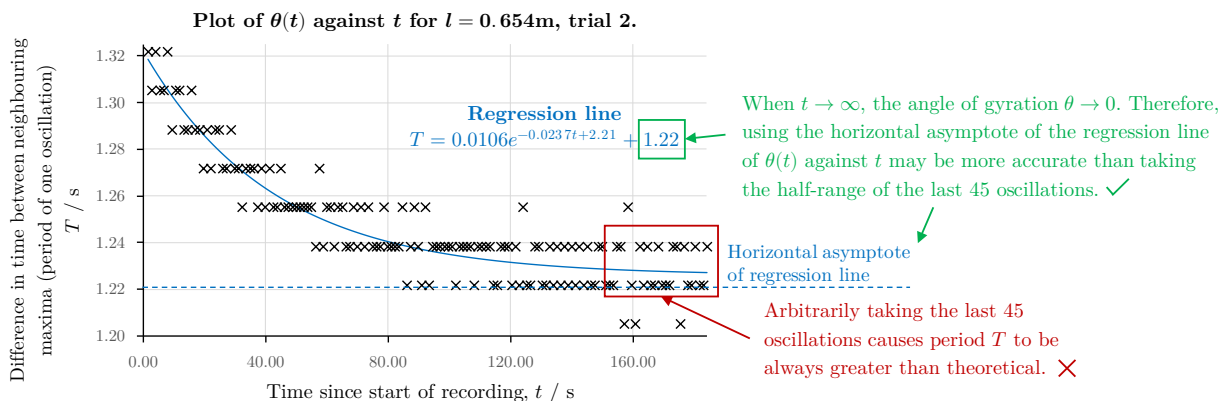


Figure 11. A demonstration of potential sources of errors and improvements.

#	Source of error	Significance	Improvements
1	Rod is released by hand, and not always released parallel to the ground, introducing chaotic motion, violating Assumption 3.	Very significant in affecting the random error. It has been observed that the bifilar pendulum is highly sensitive to small changes in the initial condition, meaning small chaotic movements initially can amplify quickly, making the measurement of period infeasible.	In Figure 11, two electromagnets should be installed on both ends of the rod and are to be controlled by a computer. This setup is less likely to introduce chaotic motion because the rods are properly levelled and released at the exact same time.
-	Initial angle of gyration $\theta_0$ is not constant across trials.	Very significant in affecting the random error. Since the dataset is obtained by the last 45 oscillations of the recording, $\theta_0$ may be different across recordings of	Instead of obtaining strictly 45 oscillations, the recordings should be first aligned such that $\theta_0$ is the same across all trials, then an intersection

	different lengths. As explored previously, nonlinearity causes the $T$ to increase as $\theta_0$ is increased.	between them should be performed to extract the overlapping sections of the recording or derived from the asymptote of $\theta(t)$ against $t$ (see Figure 12 below), maximising data reliability.
2	Orientation of the filars causes friction between the capstan and the filar, violating Assumption 2	Slightly significant in affecting the random error. Because kinetic friction is lost, the angle of gyration $\theta$ decreases at a greater rate, causing larger variations in $T$ .
3	Filars are elastic, violating Assumption 5.	Slightly significant in affecting the systematic error. Because of the weight of the rod, the length of filars $l$ can extend by a few millimetres, causing values in $T$ to be overestimated.
4	Chaotic motion can be amplified because two stands are not coupled.	Although the setup can encourage chaos in the system, the magnitude of the movement is often immeasurable, hence insignificant in affecting the random error.
-	Measurement of $T$ may be inaccurate due to errors in the Hough line detection on blurry frames	Very insignificant, as noisy data has already been filtered out by the Savitzky-Golay filter and the impact of errors have been further reduced by a large number of oscillations
		Using pendulum clamps will ensure that filars are properly secured, minimising string-to-string friction.
		Use filars with a greater spring constant to reduce the extension, thereby improving the accuracy of $l$ .
		Stability can be further increased by adding a simply supported horizontal beam between both stands, dampening chaotic motion.
		Use a camera with a greater framerate and resolution, such that when the rod is rotated at a high speed, sharper images are captured



**Figure 12.** Demonstration of using the asymptote of the regression line to find  $T$ , for  $l = 0.654\text{m}$ , trial 2.

## 15 Improvement and Extensions

Despite multiple improvements proposed above that aims to mitigate the potential sources of errors, there are still several violations to the assumptions of the equation that have not been resolved, with the most prevalent being nonlinearity (Karlin and Maday, 1985). To study this effect, the lower bound of the filar length  $l$  should be decreased so to increase the magnitude of vertical motion. Since bifilar pendulums are often used to measure the moment of inertia of aircrafts, asymmetry of the test object can lead to side-sway motion. Therefore, the representativeness of the data can be increased by testing objects other than a cylinder. Overall, to maximise the reliability of the data, the frequency and range of intervals should be increased.

## 16 Works Cited

- Amrozia, Shaheen, and Sabieh Anwar Muhammad. "A Doubly Suspended Pendulum." *LUMS School of Science and Engineering*, 2017, <https://physlab.org/wp-content/uploads/2017/05/Bifilar-Pendulum-1.compressed.pdf>.
- Canny, John. "A Computational Approach to Edge Detection." *IEEE Transactions on Pattern Analysis and Machine Intelligence*, vol. PAMI-8, no. 6, Nov. 1986, pp. 679–98. *DOI.org (Crossref)*, <https://doi.org/10.1109/TPAMI.1986.4767851>.
- Davison, C. "Bifilar Pendulum for Measuring Earth-Tilts." *Nature*, vol. 50, no. 1289, July 1894, pp. 246–49. *www.nature.com*, <https://doi.org/10.1038/050246c0>.
- Denman, H. H. "Tautochronic Bifilar Pendulum Torsion Absorbers for Reciprocating Engines." *Journal of Sound and Vibration*, vol. 159, no. 2, Dec. 1992, pp. 251–77. *DOI.org (Crossref)*, [https://doi.org/10.1016/0022-460X\(92\)90035-V](https://doi.org/10.1016/0022-460X(92)90035-V).
- Hibbeler, Russell C.. "Engineering Mechanics: Dynamics." (1986).
- Hough, Paul V. C. *Method and Means for Recognizing Complex Patterns*. US3069654A, <https://patents.google.com/patent/US3069654A/en>.
- Jardin, Matthew, and Eric Mueller. "Optimized Measurements of UAV Mass Moment of Inertia with a Bifilar Pendulum." *AIAA Guidance, Navigation and Control Conference and Exhibit*, American Institute of Aeronautics and Astronautics, 2007. *DOI.org (Crossref)*, <https://doi.org/10.2514/6.2007-6822>.
- Kane, T. R., and Gan-tai Tseng. "Dynamics of the Bifilar Pendulum." *International Journal of Mechanical Sciences*, vol. 9, no. 2, Feb. 1967, pp. 83–96. *DOI.org (Crossref)*, [https://doi.org/10.1016/0020-7403\(67\)90047-1](https://doi.org/10.1016/0020-7403(67)90047-1).
- Karlin, B. E., and C. J. Maday. "The Bifilar Pendulum: Numerical Solution to the Exact Equation of Motion." *Journal of Vibration and Acoustics*, vol. 107, no. 2, Apr. 1985, pp. 175–79. *DOI.org (Crossref)*, <https://doi.org/10.1115/1.3269241>.
- Khan, Yasir, et al. "Nonlinear Oscillation of the Bifilar Pendulum: An Analytical Approximation." *Multidiscipline Modeling in Materials and Structures*, vol. 13, no. 2, Aug. 2017, pp. 297–307. *DOI.org (Crossref)*, <https://doi.org/10.1108/MMMS-08-2016-0034>.
- Klopsteg, Paul E. "THE BIFILAR PENDULUM." *Review of Scientific Instruments*, vol. 1, no. 1, Jan. 1930, pp. 3–8. *DOI.org (Crossref)*, <https://doi.org/10.1063/1.1748636>.
- Krippendorff, Klaus. "Estimating the Reliability, Systematic Error and Random Error of Interval Data." *Educational and Psychological Measurement*, vol. 30, no. 1, Apr. 1970, pp. 61–70. *DOI.org (Crossref)*, <https://doi.org/10.1177/001316447003000105>.
- Ku, H. H. "Notes on the Use of Propagation of Error Formulas." *Journal of Research of the National Bureau of Standards, Section C: Engineering and Instrumentation*, vol. 70C, no. 4, Oct. 1966, p. 263. *DOI.org (Crossref)*, <https://doi.org/10.6028/jres.070C.025>.

- Li, Lili, et al. “Biodegradability Study on Cotton and Polyester Fabrics.” *Journal of Engineered Fibers and Fabrics*, vol. 5, no. 4, Dec. 2010, p. 155892501000500. *DOI.org (Crossref)*, <https://doi.org/10.1177/155892501000500406>.
- Matas, J., et al. “Robust Detection of Lines Using the Progressive Probabilistic Hough Transform.” *Computer Vision and Image Understanding*, vol. 78, no. 1, Apr. 2000, pp. 119–37. *DOI.org (Crossref)*, <https://doi.org/10.1006/cviu.1999.0831>.
- Mattey, R. A. *Bifilar Pendulum Technique for Determining Mass Properties of Discos Packages*. JOHNS HOPKINS UNIV LAUREL MD APPLIED PHYSICS LAB, 1 July 1974. *apps.dtic.mil*, <https://apps.dtic.mil/sti/citations/AD0787506>.
- Savitzky, Abraham., and M. J. E. Golay. “Smoothing and Differentiation of Data by Simplified Least Squares Procedures.” *Analytical Chemistry*, vol. 36, no. 8, July 1964, pp. 1627–39. *DOI.org (Crossref)*, <https://doi.org/10.1021/ac60214a047>.
- “Savitzky-Golay Smoothing Filter for Not Equally Spaced Data.” *Signal Processing Stack Exchange*, 2020, <https://dsp.stackexchange.com/a/64313>.
- Then, John W. “Bifilar Pendulum—An Experimental Study for the Advanced Laboratory.” *American Journal of Physics*, vol. 33, no. 7, July 1965, pp. 545–47. *DOI.org (Crossref)*, <https://doi.org/10.1119/1.1971900>.
- Uhler, H. S. “Period of the Bifilar Pendulum for Large Amplitudes.” *Journal of the Optical Society of America*, vol. 7, no. 3, Mar. 1923, p. 263. *DOI.org (Crossref)*, <https://doi.org/10.1364/JOSA.7.000263>.
- Weisstein, Eric W. *Moment of Inertia--Rod -- from Eric Weisstein's World of Physics*. 1996, <https://scienceworld.wolfram.com/physics/MomentofInertiaRod.html>.
- Wouter, Swart. *Bepalen van Het Massatraagheidsmoment Met Behulp van Een Bifilar Pendulum*. Technische Universiteit Delft, 2016, <https://repository.tudelft.nl/islandora/object/uuid:c275a0e4-fe21-4e27-9172-80899f463cde/datastream/OBJ/download>.

## 17 Appendix

### 17.1 Derivation of the second-order differential equation

This section aims to derive the solution to the differential equation in (6):

$$\ddot{\theta} + \frac{mgr^2}{I}\theta = 0 \quad (5)$$

Suppose the ansatz  $\theta = e^{kx}$ , then:

$$\theta = e^{kt} \quad (5.1.1)$$

$$\dot{\theta} = \frac{d}{dt}(e^{kt}) = ke^{kt} \quad (5.1.2)$$

$$\ddot{\theta} = \frac{d}{dt}(ke^{kt}) = k^2e^{kt} \quad (5.1.3)$$

Substituting (5.1.1) and (5.1.3) into (5):

$$\begin{aligned} k^2e^{kt} + \frac{mgr^2}{I}e^{kt} &= 0 \\ e^{kt} \left( k^2 + \frac{mgr^2}{I} \right) &= 0 \end{aligned} \quad (5.2)$$

In (5.2), because  $e^{kt} \neq 0$ , the characteristic equation is:

$$k^2 + \frac{mgr^2}{I} = 0 \quad (5.3)$$

Solving for  $k$ :

$$k = \pm \sqrt{\frac{mgr^2}{I}}i \quad (5.4)$$

Substituting  $k$  into the ansatz in (5.1.1):

$$\theta = e^{\pm \sqrt{\frac{mgr^2}{I}}it} \quad (5.5)$$

Applying the Euler's formula,  $e^{it} = \cos(t) + i \sin(t)$ :

$$\theta = \theta_{initial} \cos \left( \pm \sqrt{\frac{mgr^2}{I}}t \right) + \theta_{initial} i \sin \left( \pm \sqrt{\frac{mgr^2}{I}}t \right) \quad (5.6)$$

Using the initial condition of  $\theta_{initial} = \theta_0$ ,  $\dot{\theta}_{initial} = 0$ , then the solution is found to be:

$$\theta = \theta_0 \cos \left( \sqrt{\frac{mgr^2}{I}}t \right) \quad (6)$$

## 17.2 Formula for the percentage error in the period

Given the formula for a bifilar pendulum suspended by a rod:

$$T = \frac{2\pi l_{rod}}{r} \sqrt{\frac{l}{12g}} \quad (25)$$

The error in  $T$  is therefore:

$$\Delta T = \sqrt{\left(\frac{\partial T}{\partial l_{rod}} \Delta l_{rod}\right)^2 + \left(\frac{\partial T}{\partial r} \Delta r\right)^2 + \left(\frac{\partial T}{\partial l} \Delta l\right)^2}$$
$$\Delta T = \sqrt{\left(\frac{2\pi}{r} \sqrt{\frac{l}{12g}} \Delta l_{rod}\right)^2 + \left(-\frac{2\pi l_{rod}}{r^2} \sqrt{\frac{l}{12g}} \Delta r\right)^2 + \left(\frac{\pi l_{rod}}{rl} \sqrt{\frac{l}{12g}} \Delta l\right)^2} \quad (26)$$

## 17.3 Code for pilot study

Using the equation obtained in Appendix 17.1, the following code creates Fig. 3 and Fig. 4:

Filename: pilot.py

Language: Python 3.9.7

Packages used:

- numpy 1.8.5
- pandas 1.1.2
- matplotlib 2.2.5

```
'''
This script does the following:
- calculate T for 0.001 < l < 1.500, with increments of 0.001
- save the raw data to a CSV file.
- for 0.001 < l < 1.500, with increments of 0.001:
    - for 0.0010 < r < 0.0979, with increments of 0.0001:
        - calculate the percentage error in T
        - plot on a 2D axis with the 'turbo' colormap
- store the graph in a PNG image.
'''

import math
import numpy as np
import matplotlib.pyplot as plt
import pandas as pd

g = 9.81

def getT(l_rod, r, l):
    return 2*math.pi*l_rod/r*math.sqrt(l/12/g)

def getTerr(l_rod, delta_l_rod, r, delta_r, l, delta_l):
    return math.sqrt(
        math.pow((delta_l_rod*math.pi*math.sqrt(l/g)) / (math.sqrt(3)*r), 2) +
        math.pow((delta_r*math.pi*l_rod*math.sqrt(l/g)) / (math.sqrt(3)*math.pow(r, 2)), 2) +
        math.pow((delta_l*math.pi*l_rod*math.sqrt(l/g)) / (math.sqrt(3)*r*l*2), 2)
    )

df0 = pd.DataFrame([(l, getT(.1958, .075, l)) for l in np.arange(.001, 1.500, .001)], columns=['l', 'T'])
df0.to_csv('output1/pilot.csv', index=False)
```



```

data = []
l_rod,  $\delta l_{rod}$  = .1958, .0001
 $\delta l$  = .001
 $\delta r$  = .001
for l in np.arange(.001, 1.500, .001):
    for r in np.arange(.001, .0979, .0001):
        pct $\delta T$  = min(getTerr(l_rod,  $\delta l_{rod}$ , r,  $\delta r$ , l,  $\delta l$ ) / getT(l_rod, r, l), .025)
        data.append([l, r, pct $\delta T$ ])

df = pd.DataFrame(data, columns=['l', 'r', 'pct $\delta T$ '])
plt.rcParams['font.family'] = 'Latin Modern Roman'
plt.scatter(x=df['l'], y=df['r'], c=df['pct $\delta T$ '], cmap='turbo')
plt.xlim([.001, 1.500])
plt.ylim([.001, .0979])
plt.savefig('output1/pilot.png', dpi=300)

```

## 17.4 Formula for the adjustment of filar length

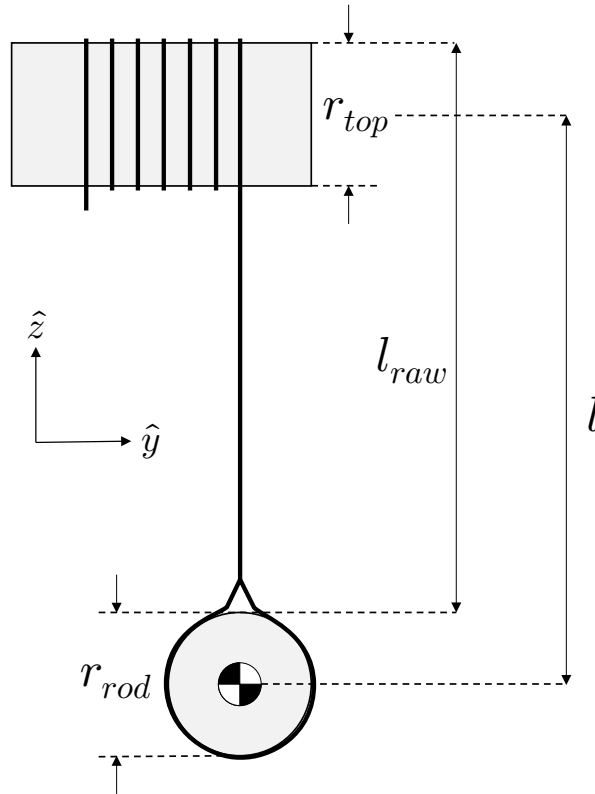


**Figure \***. The cross-sectional view of the setup along the  $\hat{y}$ - $\hat{z}$  plane.

In the experiment, the raw filar length ( $l_{raw}$ ) is measured by resting a metre ruler on the top of the rod and reading the value on the top of the top rod, as demonstrated in the figure above. Hence, the true filar length is better represented by:

$l$  = raw filar length – distance to centre of top rod + distance to centre of mass of rod

$$l = \text{raw filar length} - \frac{\text{diameter of top rod}}{2} + \frac{\text{diameter of rod}}{2}$$

$$l = l_{raw} - \frac{1}{2}d_{top} + \frac{1}{2}d_{rod} \quad (11)$$

## 17.5 Code for parsing raw video

Filename: parse.py

Language: Python 3.9.7

Packages used:

- rich 9.10.0
- numpy 1.8.5
- pandas 1.1.2
- opencv-python 4.5.3.56

```
'''
This script does the following:
- read the list of videos from a specific folder
- for each video, process each frame:
  - for each frame, convert the frame to greyscale
  - perform canny edge detection
  - perform probabilistic hough line transform
  - for each possible location of the rod:
    - select the longest line
    - calculate the length of the rod (in pixels) using Pythagoras\
    - calculate the angle of the rod (in radians) using atan2
  - aggregate the temporal changes of the rod
- store the data in multiple CSV files for further processing
'''

from rich.progress import Progress
import numpy as np
import pandas as pd
import cv2
import os

class Line:
    def __init__(self, line):
        self.p1 = np.array(line[0][:2]).astype(int)
        self.p2 = np.array(line[0][2:4]).astype(int)

    def getLen(self):
        self.length = np.sqrt(np.sum((self.p1 - self.p2) ** 2, axis=0))
        return self

    def getAngle(self):
        self.angle = np.arctan2(
            self.p2[1] - self.p1[1],
            self.p2[0] - self.p1[0] if self.p1[0] < self.p2[0] else self.p1[0] - self.p2[0]
        )
        return self

with Progress() as progress:
    files = os.listdir('src')
    task0 = progress.add_task(f"[green]Processing files...", total=len(files))
    for filename in files: # process each video in the specified folder
        progress.update(task0, advance=1, description=f"[green]Processing {filename}...")
        capture = cv2.VideoCapture(os.path.join("src", filename))

        totalframecount = int(capture.get(cv2.CAP_PROP_FRAME_COUNT))
        task1 = progress.add_task(f"[green]Parsing frames...", total=totalframecount)
        vals, framecount = [], 0
        while 1:
            success, frame = capture.read()
            if not success:
                break

            image = cv2.cvtColor(frame, cv2.COLOR_BGR2GRAY)
            edges = cv2.Canny(image, 100, 100, L2gradient=True)
```

```

        lines = cv2.HoughLinesP(edges, 1, np.pi/180, 100, maxLineGap=200)

        if lines is not None:
            l = Line(sorted(lines, key=lambda x:Line(x).getLen().length, reverse=True)[0]).getLen().getAngle()

            vals.append([framecount, l.length, l.angle])

        progress.update(task1, advance=1)
        framecount += 1

df = pd.DataFrame(vals, columns=['frame', 'length', 'angle'])
df.to_csv(os.path.join('output', f'{os.path.splitext(filename)[0]}.csv'), index=False)

```

## 17.6 Code for parsing raw data

Filename: analyse.py<sup>9</sup>

Language: Python 3.9.7

Packages used:

- rich 9.10.0
- numpy 1.8.5
- pandas 1.1.2
- scipy 1.18.5

```

'''
This script does the following:
- read raw data from a specific folder
- for each raw data
    - smoothen noisy data using a non-uniform Savitzky-Golay filter
    - obtain the peaks of the smoothened data
    - for each peak:
        - calculate the average time
        - calculate the difference in time
        - calculate the average length of the rod (in pixels)
        - calculate the average angle of the rod (in radians)
- aggregate all processed data
- store the data in one CSV file for further processing
'''

import os
import numpy as np
import pandas as pd
from scipy.signal import argrelextrema
from rich.progress import Progress

def non_uniform_savgol_filter(x, y, window, polynom):
    half_window = window // 2
    polynom += 1

    A = np.empty((window, polynom))
    tA = np.empty((polynom, window))
    t = np.empty(window)
    y_smoothed = np.full(len(y), np.nan)

    for i in range(half_window, len(x) - half_window, 1):
        for j in range(0, window, 1):
            t[j] = x[i + j - half_window] - x[i]

        for j in range(0, window, 1):
            r = 1.0

```

<sup>9</sup> The code for the non-uniform Savitzky-Golay filter is obtained from <https://dsp.stackexchange.com/a/64313>. (Signal Processing Stack Exchange, 2020)

```

        for k in range(0, polynom, 1):
            A[j, k] = r
            tA[k, j] = r
            r *= t[j]

    tAA = np.matmul(tA, A)
    tAA = np.linalg.inv(tAA)
    coeffs = np.matmul(tAA, tA)

    y_smoothed[i] = 0
    for j in range(0, window, 1):
        y_smoothed[i] += coeffs[0, j] * y[i + j - half_window]

    if i == half_window:
        first_coeffs = np.zeros(polynom)
        for j in range(0, window, 1):
            for k in range(polynom):
                first_coeffs[k] += coeffs[k, j] * y[j]
    elif i == len(x) - half_window - 1:
        last_coeffs = np.zeros(polynom)
        for j in range(0, window, 1):
            for k in range(polynom):
                last_coeffs[k] += coeffs[k, j] * y[len(y) - window + j]

    for i in range(0, half_window, 1):
        y_smoothed[i] = 0
        x_i = 1
        for j in range(0, polynom, 1):
            y_smoothed[i] += first_coeffs[j] * x_i
            x_i *= x[i] - x[half_window]

    for i in range(len(x) - half_window, len(x), 1):
        y_smoothed[i] = 0
        x_i = 1
        for j in range(0, polynom, 1):
            y_smoothed[i] += last_coeffs[j] * x_i
            x_i *= x[i] - x[-half_window - 1]

    return y_smoothed

df2s = []
with Progress() as progress:
    files = os.listdir('output')
    task = progress.add_task(f"[green]Processing files...", total=len(files))
    for filename in files:
        progress.update(task, advance=1, description=f'[green]Processing {filename}...')
        df = pd.read_csv(os.path.join("output", filename))
        smoothed = non_uniform_savgol_filter(df.frame.values, df.angle.values, 31, 5)
        idx = argrelextrema(smoothed, np.greater, order=5)[0]

        df1 = pd.DataFrame(columns=["frame", "length", "turning_smoothed"])
        df1['frame'] = df.iloc[idx].frame
        df1['length'] = df.iloc[idx].length
        df1['turning_smoothed'] = smoothed[idx]

        df1l, df2l = df1.values.tolist(), []
        for i, j in enumerate(df1l[:-1]):
            r0, r1 = df1l[i], df1l[i+1]
            df2l.append([
                (r1[0] + r0[0]) / 2 / 60,
                (r1[0] - r0[0]) / 60,
                (r1[1] + r0[1]) / 2,
                (r1[2] + r1[2]) / 2
            ])

        identifier = os.path.splitext(filename)[0]
        df2s.append(pd.DataFrame(df2l, columns=[

```

```

        f"{identifier}_avg_frame",
        f"{identifier}_frame_diff",
        f"{identifier}_avg_length",
        f"{identifier}_avg_turning_smoothed"
    )))

df2 = pd.concat(df2s, axis=1)
df2.to_csv(os.path.join("output1", "all.csv"), index=False)

```

## 17.7 Code for numerical integration of exact nonlinear equation

Filename: simulate.py

Language: Python 3.9.7

Packages used:

- numpy 1.8.5
- pandas 1.1.2
- scipy 1.18.5

```

'''
This script does the following:
- for 0 m < l < 1.5 m in increments of 0.001 m:
    - for initial  $\theta \rightarrow 0, \pi/12, \pi/6, \pi/4, \pi/3$  and  $5\pi/12$ :
        - numerically solves the exact nonlinear equation from  $0 < t < 20$ , with step size 0.001s
        - derives the period of the motion by averaging the  $\Delta t$  in the peaks of  $\theta(t)$ 
- saves the results to a CSV file.
'''

from scipy.integrate import odeint
from scipy.signal import argrelextrema
import numpy as np
import pandas as pd

g = 9.81
r = 0.0750
l_rod = 0.1958

def theta_nonlinear(U, x):
    return [U[1], -3*g*np.power(2*r,2)/(1*np.power(l_rod,2))*np.sin(U[0])/np.sqrt(1-0.5*np.power(2*r/l, 2)*(1-np.cos(U[0])))]

def theta_linear(U, x):
    return [U[1], -12*g*np.power(r,2)/(1*np.power(l_rod,2))*U[0]]

data = []
for sqrt_l in np.linspace(0, 1.5, 1500):
    l = np.power(sqrt_l, 2)
    row = [sqrt_l]
    for n in [0.0001, 1, 2, 3, 4, 5]:
        xs = np.linspace(0, 20, 20000)
        ys = odeint(theta_nonlinear, [n*np.pi/12, 0], xs)[: ,0]

        row.append(np.mean(np.diff(xs[argrelextrema(ys, np.greater, order=5)[0]])))
    data.append(row)

df = pd.DataFrame(data, columns=['sqrt_l', '0', 'pi/12', 'pi/6', 'pi/4', 'pi/3', '5pi/12'])
df.to_csv('output1/simulate.csv')

```